Bilateral Alignment of Receptive Fields in the Olfactory Cortex Points to Non-Random Connectivity

Julien Grimaud[1,2,4], William Dorrell[3,4], Cengiz Pehlevan[3,4], and Venkatesh Murthy[2,4]*.
[1] Molecules, Cells, and Organisms Graduate Program, Harvard University, Cambridge, Massachusetts, USA.
[2] Department of Molecular and Cellular Biology and Center for Brain Science, Harvard University, Cambridge, Massachusetts, USA.
[3] John A. Paulson School of Engineering and Applied Sciences, Harvard University, Cambridge, Massachusetts, USA.
[4] Center for Brain Science, Harvard University, Cambridge, Massachusetts, USA
*Lead Author. Correspondence: vnmurthy@fas.harvard.edu

Abstract

While olfactory sensory neurons expressing the same receptor in the nose converge to the same location in olfactory bulb, projections from the olfactory bulb to the cortex exhibit no recognizable spatial topography. This lack of topography is thought to carry over for interhemispheric connectivity, which originates cortically. If connections to and within the cortex are random, information reaching a cortical neuron from both nostrils will be uncorrelated. Instead, we found that the odor responses of individual neurons to stimulation of both nostrils are highly matched. More surprisingly, odor identity decoding optimized with information arriving from one nostril transfers very well to the other side. Computational analysis shows that such matched odor tuning is incompatible with random connections, but is explained readily by local Hebbian plasticity. Our data reveal that despite the distributed nature of the sensory representation in the olfactory cortex, odor information across the two hemispheres is highly coordinated.

Introduction

In many mammalian brain areas, neurons physically close to each other respond to cues that are also close to each other in their sensory space, leading to topographic representations (Kaas, 1997). While this ordering principle is common in vision, audition and somatosensation (Brewer and Barton, 2016; Harding-Forrester and Feldman, 2018; Nauhaus and Nielsen, 2014), olfaction appears to be an exception, with seemingly unstructured representations (Caron et al., 2013; Giessel and Datta, 2014). How a coherent representation of odorants arises in the olfactory cortex in the face of disorder, remains an open question.

Odors are detected by sensory neurons embedded in the olfactory epithelium within the nose. The odor information, converted into action potentials, then reaches the olfactory bulbs (OB), which send information to the olfactory cortex (OC). The OC includes the anterior olfactory nucleus (AON) and the anterior and posterior piriform cortices (APC and PPC, respectively) (Giessel and Datta, 2014; Mori, 1999; Nagayama et al., 2014; Wilson and Sullivan, 2011).

Projections from the olfactory epithelium to the OB preserve coarse information about spatial position, and their destinations on the surface of the OB, the glomeruli, are found in predictable locations (Soucy et al., 2009; Strotmann et al., 2000). While there may be some functional organization in the glomerular layer (Mori, 1999; Murthy, 2011; Strotmann et al., 2000), whatever order present in the OB appears to be largely lost in the OC (Bekkers and Suzuki, 2013; Ghosh et al., 2011; Miyamichi et al., 2011; Sosulski et al., 2011; Wilson and Sullivan, 2011) (Figure 1A). This lack of apparent structure led to the prevalent view that OC projections are structurally random, each OC neuron receiving an arbitrary set of OB inputs (Bekkers and Suzuki, 2013; Choi et al., 2011; Davison and Ehlers, 2011; Ghosh et al., 2011; Kay, 2011; Miyamichi et al., 2011; Schaffer et al., 2018; Sosulski et al., 2011; Wilson and Sullivan, 2011).

In many species, including rodents, a septum separates the two nares, and inhaled odors are physically compartmentalized within each nostril (Kikuta et al., 2008). Hence the crossover between both sides of the olfactory system is exclusively neural (Bekkers and Suzuki, 2013; Wilson and Sullivan, 2011). Additionally, since the OB does not send contralateral projections, inter-hemispheric projections originate exclusively from the OC (Boyd et al., 2012; Haberly and Price, 1978; Kikuta et al., 2008; Scott et al., 1980). Consequently, the lack of apparent structure in the OC should propagate across hemispheres (Schaffer et al., 2018) (Figure 1A). In other words, the prevalent view of OC connectivity being random must apply to bilateral projections.

The seemingly random pattern of connectivity may preclude precise matching of connections from the right and the left sides of the olfactory system. However, several studies suggest at least some level of coordination between the two brain hemispheres. First, despite the prevalent

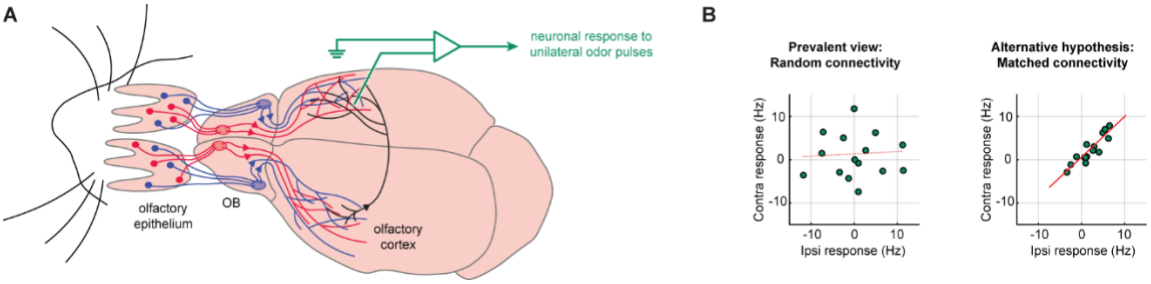

Figure 1: Bilateral Olfactory Circuitry and Projection Pattern. (A) Topographic organization of the olfactory system, diagram. Glomeruli at the surface of the OB are found at predictable locations. Glomerular maps appear to be largely lost in the OC. This lack of apparent structure led to the prevalent view that OC projections are random, each OC neuron responding to an arbitrary set of odor objects. (B) Hypotheses tested in the present study. If the OB projections arriving to the OC are truly random (left), we expect to see little match between the ipsi- and contralateral odor tunings of cortical neurons. Alternatively, if bilateral OC projections are structured (right), we expect matched bilateral odor tuning. Further description of panel (B) can be found in Figure 4A.

asymmetry of the airflow coming into the two nostrils, there is an apparent perceptual constancy (Bojsen-Moller and Fahrenkrug, 1971; Eccles, 2000; Kikuta et al., 2008). Second, rats trained to associate odors delivered to one nostril with a reward could recall these associations if odors were delivered to the other nostril (Kucharski and Hall, 1987, 1988). Humans have a similar ability (Mainland et al., 2002).

From the above discussion, it seems challenging to reconcile the dominant view of random OC connectivity, with behavioral studies suggesting bilaterally-stable odor experience. However, some tantalizing hints exist. For example, there is some evidence for responses in olfactory cortical areas to contralateral odor stimulation, but it is limited by the number of neurons reported and a lack of comparison of ipsi- vs contralateral stimulation (Kikuta et al., 2008, 2010; Wilson, 1997). More recently, it was shown that despite the apparent randomness of the OB-OC projections, the piriform cortex could partially retain the olfactory map overlap present in the OB, allowing the OC in each hemisphere to perform similar odor generalization operations (Babadi and Sompolinsky, 2014; Schaffer et al., 2018).

In this study, we challenged the prevalent view of OC connectivity by comparing the bilateral odor tuning of individual neurons in the OC of mice. If inter-hemispheric projections were truly random, one would expect little to no relationship between the way the OC responds to ipsilateral and contralateral odor presentations (Figure 1B, left). Alternatively, bilaterally matched odor responses in the OC (Figure 1B, right) would point non-random connectivity.

Results

A New Method for Unilateral Odor Delivery

A main goal of this study was to compare the bilateral odor receptive fields of OC neurons of awake mice. To do so, we needed a way to reliably deliver odor puffs to one nostril at a time. Previous studies have used two different techniques to achieve such unilateral odor stimulations. Either a piece of tubing was inserted in each nostril (Wilson, 1997), or the two nostrils were separated by a plastic septum (Kikuta et al., 2008, 2010). Since mice have a very sensitive muzzle, neither of these approaches is applicable to awake animals.

We developed a new facial mask for unilateral odor delivery in awake mice (Figure 2A). On each side of the mask, close to the nostrils, we used a computer-controlled olfactometer to deliver 15 monomolecular odors, one at the time, to the left or the right nostril (Figures S1A-S1B). The mask was connected to an airflow sensor for respiration monitoring (Figures S1C-S1F). We aligned all neuronal odor-evoked activity to the first sniff after odor onset (see Methods).

We tested the side selectivity of the mask through two methods. First, we simultaneously monitored the glomerular activity at the surface of the OBs of OMP-GCaMP3 mice (Isogai et al., 2011) through calcium imaging, while delivering odors to either nostril (Figure 2B) (n=155 glomeruli, 6 OBs, 3 mice). When odors were presented on the contralateral nostril, glomeruli showed little to no response (Figures 2C-2E).

We also performed extracellular recordings of mitral/tufted cells (M/T) in the OB of awake mice using chronically-implanted tetrodes (n=42 single units isolated from 4 mice) (Figure 2F, S1G-S1J, and Table S1). We observed little M/T response to contralateral presentations:

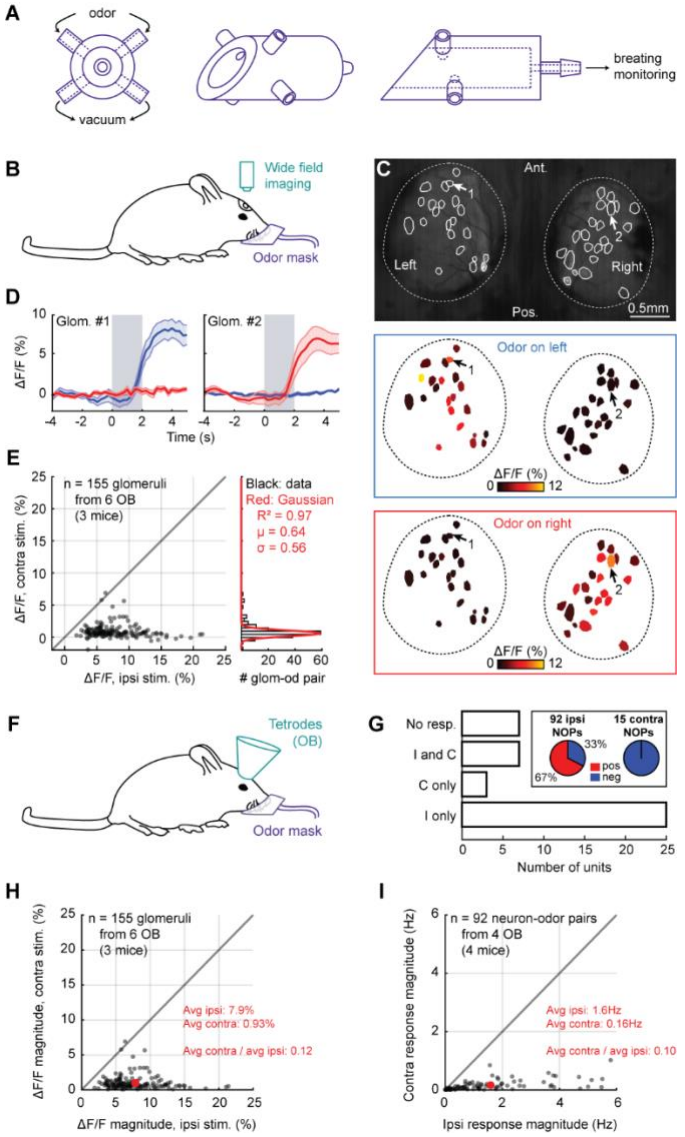

Figure 2: A New Method for Unilateral Odor Delivery. (A) Diagram of the odor mask. From left to right: front, rotated, and side view. (B) Calcium imaging setup. (C) Exemplar glomerular activity. Example: all glomeruli from OB1, isopropyl tiglate. Arrows: see below. (D) Exemplar glomerular activity over time. Grey: odor on (here: isopropyl tiglate). Blue: odor on the left nostril. Red: odor on the right nostril. Average ± SEM. Glomeruli 1 and 2 correspond to arrows 1 and 2 in panel 1C. (E) Glomerular responses. Each dot is the response of one glomerulus to one odor (glom-od pair). Histogram: contralateral responses. Red: Gaussian fit. (F) Tetrode recording setup. (G) Unilateral response profile of M/T cells. NOP: neuron-odor pair. (H) Magnitude of glomerular response. Red: average for each side. (I) Magnitude of M/T cell response. Only the ipsilaterally responding NOPs are shown. Red: average for each side.

out of the 42 isolated neurons, 32 responded to ipsilateral stimulations, while 10 showed significant contralateral responses (Figure 2G). Furthermore, while the ipsilateral M/T cell responses were largely positive, the few contralateral responses were always negative (Figure 2G).

Finally, we quantified the ratio of ipsi to contralateral response magnitude elicited by the mask. This ratio was 0.12 in our glomerular imaging data (Figure 2H) and 0.10 in our M/T recordings (Figure 2I). Therefore, on average, odor responses were 8 to 10 times stronger on the ipsilateral side of the mask, compared to the contralateral side.

These observations probably overestimate the crossover of the mask, since the weaker responses we reported may be due to changes in spontaneous activity rather than odor-evoked responses. Previous work has indicated that M/T cell responses to 0.1% odors were quite similar to 1% odors (Bolding and Franks, 2017, 2018). Since M/T cell responses are substantially smaller to contralateral presentation, the effective odor concentration in the ipsilateral nostril, when odors are presented contralaterally, is likely to be much less than 10%.

Together, these results confirmed that odors, when delivered to one nostril through our custom-built mask, activate sensory neurons in the other nostril at least an order of magnitude less than ipsilateral activation.

Unilateral Odor Tuning of Different Regions of the Olfactory Cortex

We next used our unilateral odor delivery system to characterize how the OC responds to unilateral odor presentations. To do so, we monitored the activity of the OC through extracellular recordings in awake mice (n=10 mice, 1830 neurons total; AON: 3 mice, 384 neurons; APC: 4 mice, 931 neurons; PPC: 3 mice, 505 neurons) (Figures 3A, S2, and Table S1).

Overall, neurons in the OC had weak spontaneous activity (Figure 3B), in accordance with previous studies (Bolding and Franks, 2017; Litaudon et al., 2003; Zhan and Luo, 2010). Spontaneous activity in the AON was significantly higher than in the piriform cortex (Kruskal-Wallis test: p<0.0001; post-hoc rank-sum test: AON versus APC, p<0.0001; AON versus PPC, p=6.3e-3; APC versus PPC, p=0.33).

We found a diversity of responses to ipsi- as well as contralateral odor stimulation in all three OC areas, including neurons that responded to odors presented to either one or the other nostril, or to both nostrils (Figures 3C-3D). Importantly, in all three OC regions, a sizeable fraction of neurons responded to contralateral odor presentations (Fraction of neurons significantly responding to at least one odor presented on the ipsilateral nostril, AON: 86%; APC: 81%; PPC: 80%; contralateral side, AON: 87%; APC: 83%; PPC: 80%), expanding earlier anesthetized observations to the awake OC (Kikuta et al., 2008, 2010; Wilson, 1997).

OC neurons typically responded to at most a few odors from our odor panel (Figure 3E), as previously reported with bilateral odor stimulations (Bolding and Franks, 2017; Iurilli and Datta, 2017). We found a wide range of response magnitudes across the OC, and contralateral responses were largely as strong as ipsilateral ones (Figure 3F; Wilcoxon signed-rank test, ipsi versus contra distribution, AON: p=8.2e-3; APC: p=0.94; PPC: p=0.40).

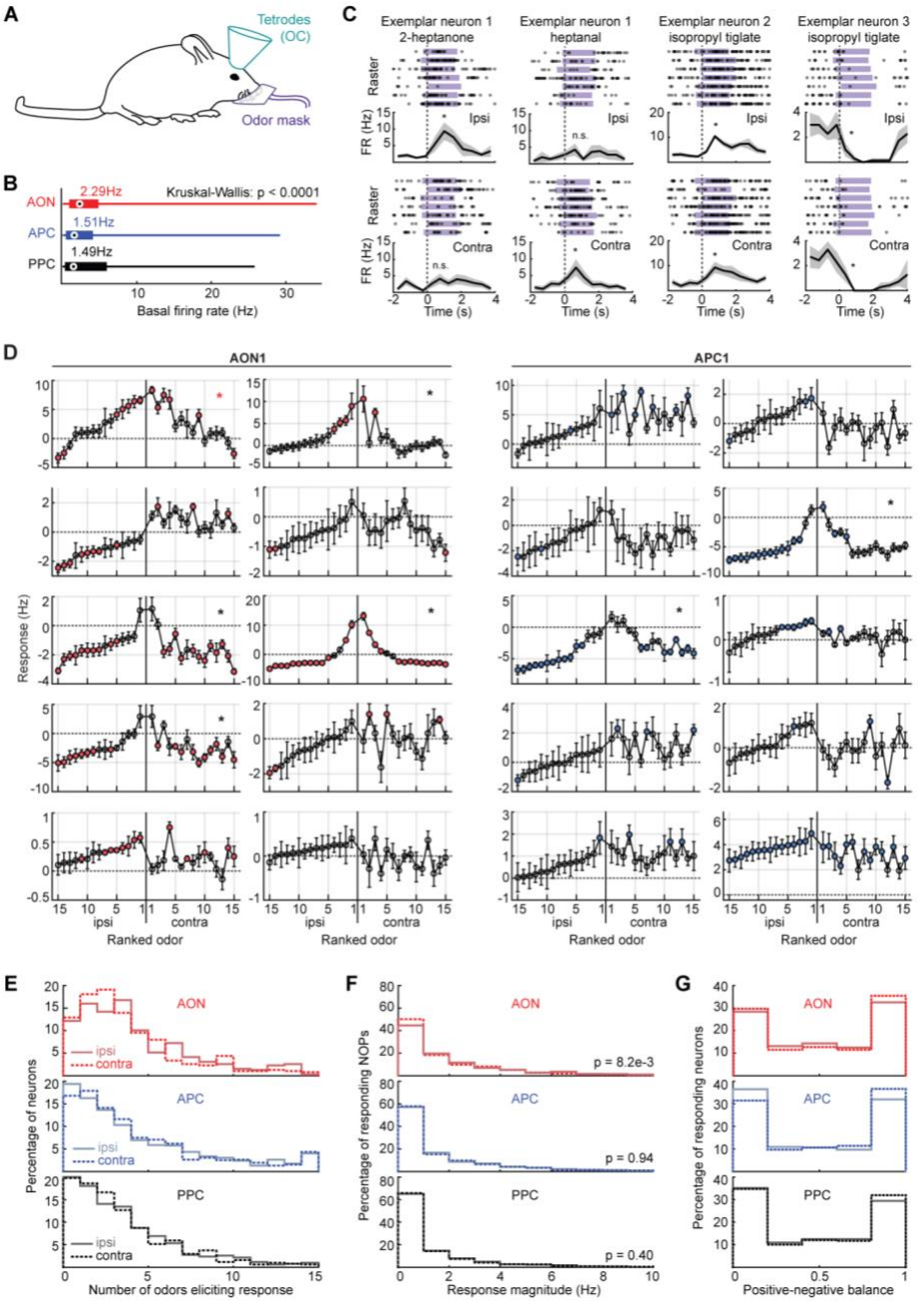

Figure 3: Odor Receptive Fields of Neurons in the Olfactory Cortex. (A) Experimental setup. (B) Basal activity per region. Circle and value next to it: median. Thick bar: quartiles. Thin bar: range of values. (C) Exemplar odor responses over time. Purple: odor delivery. Responses were aligned to the first sniff following odor onset (dotted line). PSTH: average ± SEM. Examples taken from APC1. (D) Odor responses, illustration. Neurons randomly picked from AON1 (left) and APC2 (right). For each neuron, odors were ranked based on the response magnitude to ipsilateral presentations, which are shown in the left half of each plot. The contralateral responses are then shown with the same rank order of odors for each neuron. Each dot gives the average response ± SEM across the 7 trials, and significant responses are colored red. Asterisk: the ipsi- and contralateral tuning curves of these neurons are visually similar. Further analysis shows that their odor responses are bilaterally correlated. See Figure 4A for details. (E) Distribution of the number of odors eliciting a response in a given neuron, shown for three regions and for ispi- and contra-lateral stimulation. (F) Distribution of response magnitudes (only significant ones) for all neurons and odors in three regions and for both sides. (G) Positive-negative balance per region and side. 0 = all negative significant responses; 1 = all positive.

An idiosyncratic feature of olfactory cortical responses is that a neuron that responds to a particular odor with an increase in firing rate, tends to exhibit increases in firing rates for any other odor it responds to; similarly, a neuron having inhibitory response to an odor

is also inhibited by any other odor it responds to (Bolding and Franks, 2017; Hu et al., 2017; Kikuta et al., 2008; Otazu et al., 2015; Zhan and Luo, 2010). We find that this feature applies to all three cortical regions we examined (Figure 3G).

Overall, in all OC regions recorded, we found reliable unilateral odor responses to both the ipsi- and contralateral nostrils.

Strong Bilateral Correlations in the Olfactory Cortex

Our data indicate that the OC receives robust contralateral odor information, but it is unclear whether this information is similar to that arriving ipsilaterally. To examine this issue, we related the average odor-evoked responses to ipsilateral against contralateral presentations.

First, we plotted the ipsi- versus contralateral odor responses for each neuron individually. Given the prevalent view of OC connectivity, we expected OC neurons to show little to no match between their ipsi- and contralateral odor response profiles. To our surprise, we found many neurons with bilaterally-correlated odor responses (Figure 4A) (F-test, significance of the linear model, from left to right neuron, top row: p=0.41; p=0.84; p=0.54; p=0.59; bottom row: p=5.3e-6; p=5.5e-4; p=6.6e-3; p=2.2e-4) (see also Figure 3D, neurons with an asterisk). We used a bootstrap strategy to determine that the percentages of bilaterally-correlated neurons were significantly higher than what one would expect from chance in the AON and APC, but not PPC (Figures 4B, 4C, and S3A-S3D). Bilateral correlations were strong (Figure 4D), with mostly positive slopes (Figure 4E), and a distribution of intercepts centered on zero (Figure 4F).

We wondered if the bilaterally matched responses occurred preferentially in a particular neuron type. We used a classic method for identifying putative excitatory and inhibitory neurons – the width of extracellular action potentials (Frank et al., 2001; Gur et al., 1999; Hassani et al., 2009; Povysheva et al., 2006; Suzuki and Smith, 1985; Swadlow, 2003; Weir et al., 2015). Most of the bilaterally-correlated neurons in the AON and APC had a broad spike with lower spontaneous activity (Figure S3E-S3H), suggesting their putative excitatory nature.

Finally, we compared the ipsilateral and contralateral population representation in the three OC regions recorded for each odor (Figures 4G and S4A-S4C). Consistent with our analysis of individual bilaterally-correlated neurons, we found that unilateral population representations were significantly and strongly correlated for all odors tested in the AON and APC, but not PPC (Figures S4A-S4E) (see Table S2 for detailed statistics). When considering each mouse separately, our conclusions held true for most odors (Figure S4F).

Together, these data indicate that the odor information arriving contralaterally to the OC strongly match that arriving (more directly) ipsilaterally, at least in the first stages of odor processing (AON and APC).

Accurate Decoding of Odor Identity from Contralateral Activity

Odor selectivity in the OC allows a population representation of odor identity, and odor identity can be decoded from the activity of a sufficient number of neurons (Bolding and Franks, 2017). If odor responses are similar for ipsi- and contralateral presentations, decoding of identity should be transferrable. To formally test this, we asked a linear classifier to decode odor identity from OC responses to

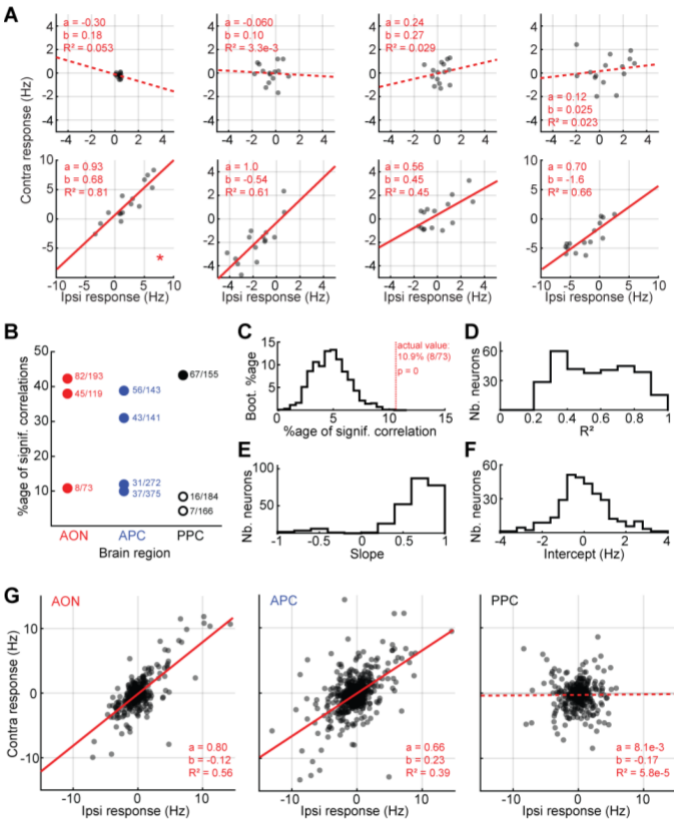

Figure 4: Side-Invariant Odor Responses in the Olfactory Cortex. For panels (A) and (G), red line: linear regression (contra = a x ipsi + b). Solid lines show significant regressions (F-test, p < 5%). (A) Exemplar ipsi- versus contralateral responses per neuron. Examples picked from AON1. Each dot is a different odor. The neurons in the bottom panels are bilaterally-correlated. Asterisk: same neuron as in Figure 3D, left panel, red asterisk. (B) Percentage of bilaterally-correlated neurons (BCNs) per mouse. Each dot is a mouse. Fractions next to each dot: number of BCNs / total number of neurons. Full circle: the fraction is significantly higher than chance. The mice with lower percentage of BNCs were usually the ones in which neurons responded to fewer odors on average (Figure S6). (C) Significance of the percentages of BCNs. Here we show the distribution of chance percentages for AON1, obtained with a bootstrapping procedure. (D) to (F) Coefficients of determination, slopes, and intercepts of the BCNs in the AON and APC (Nb: number). (G) Ipsi- versus contralateral responses per region for odor 1 (isopropyl tiglate). Each dot represents one neuron. For the equivalent graphs across all odors, see Figure S4.

one nostril, after we trained it with OC responses to the opposite nostril.

In brief, at each instance we created a training set by randomly removing one trial per odor (Bolding and Franks, 2017). If we were testing on the same side as we trained (e.g. train ipsilaterally, test ipsilaterally), then we tested the classifier on the trials outside of the training set. If we were testing on the opposite side (e.g. train ipsilaterally, test contralaterally), then one trial per odor from the opposite side was randomly chosen to form the test set (Figure 5A). We performed all our decoding analyses over an odor response window of 2s, as it maximized performance of odor decoding on the same side (Figure S5A).

In all three cortical regions assessed, the decoder performed with similarly high levels of accuracy when tested on data from the same or the opposite side (Figures 5B-5C). In other words, odor identity decoding optimized with responses to stimulation from one nostril transfers very well to stimulation of the other side. Note that the

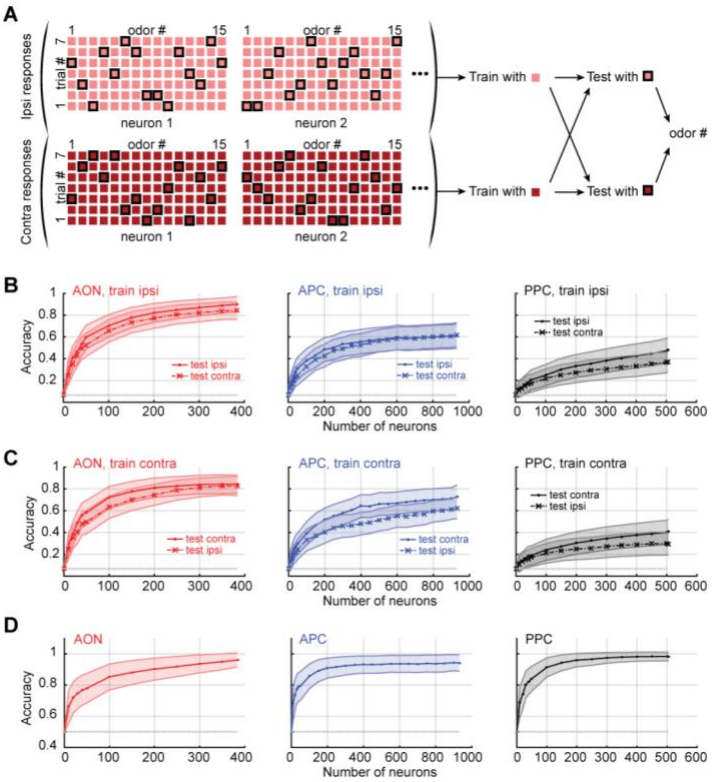

Figure 5: Decoding Contralateral Odor Identity. (A) Diagram of the odor decoding process. (B) and (C) Odor identity decoding per region. Mean ± SEM over 200 repetitions of the decoding process. For (B), the decoder was trained with data from ipsilateral presentations. For (C), the decoder was trained on contralateral odor responses. (D) Side identity decoding per region. Mean ± SEM over 200 repetitions of the decoding process. For (B) to (D), grey dotted line: chance.

seemingly decrease of decoding performance in more posterior cortical regions is due to variability across mice (Figure S5B). More precisely, mice with overall weaker and fewer odor-evoked responses showed lower odor decoding performances, no matter the side tested (Figure S6).

Rodents are able to determine the direction of the odor stimulation at short distances (Esquivelzeta Rabell et al., 2017; Rajan, 2006). We asked whether population activity in a single hemisphere differs sufficiently for stimulation of ipsi- and contralateral nostril to allow decoding of intensity differences between the two sides. Side identity could indeed be decoded with high accuracy (Figure 5D), which confirms that odor representations from both sides, despite similarities, remain distinct and separable.

Together, our data indicate that odor decoding is transferrable across sides. Ipsi- and contralateral odor representations, while distinct, share a high degree of similarity.

A Computational Model of Bilateral Matching in the Olfactory Cortex

A prevalent view is that the projections to the OC is distributed and random. Can this apparent randomness explain the high degree of bilateral matching we found in the OC? Previous work has shown that, if two correlated representations are projected through the same random matrix, the resulting representations remain correlated (Babadi and Sompolinsky, 2014; Schaffer et al., 2018). However, this model does not fully recapitulate bilateral olfactory circuitry, as the information coming from each nostril passes through a different set of seemingly random projections (Figure 1A).

To address this limitation, we implemented a computational model of the olfactory system to test matching of ipsilateral and contralateral odor tuning in the OC as a function of structure in bilateral projections (Figure 6A). In brief, we simulated two odor-evoked cortical representations (one for each brain hemisphere) and linked them with a cross-cortical connectivity matrix G. This matrix was part-random, with elements drawn from a Gaussian distribution (G_{Random}), and part-Hebbian, linking the same-odor representations in each hemisphere together ($G_{Structured}$). Explicitly:

$$G = \alpha G_{\text{Structured}} + (1-\alpha) G_{\text{Random}}$$

Parameter α took values between 0 and 1 with $\alpha = 0$ corresponding to purely random connectivity and $\alpha = 1$ to purely structured connectivity. The random and Hebbian components were scaled appropriately to have α represent the proportion of contralateral input magnitude that is formed by structured connectivity.

We first validated our model by comparing the ipsilateral (Figures S7A-S7C) and contralateral (Figures 6B-6D) simulated odor responses with the actual neuronal responses. Our model appears to replicate the statistics of neuronal responses remarkably well, with minimal adjustments of the model parameters (see Methods).

Then we computed four measurements from our modeled OC while varying α, the parameter that controls cross-hemispheric structured connectivity: the overall correlation of odor population representation across sides (Figures 6E-6F; similar to Figure 4G), the fraction of bilaterally-correlated neurons (Figure 6G; similar to Figure 4B), the accuracy of odor identity decoding (Figures 6H-6I and S7D; similar to Figures 5B-5C), and the accuracy of side identity decoding (Figure 6J; similar to Figure 5D).

The four computed measurements best match our actual AON neuronal recordings with a non-zero α (approximately 0.4). This result does not vary when we change the size of the modeled OC population (Figures S7E-S7H). Further, we provide an analytical derivation showing that interhemispheric correlations cannot arise from a null α (Note S1).

Together, these results suggest that random projections alone cannot explain our OC results. The bilateral projections must be structured.

Discussion

In many animals, odor information collected by the two nostrils remains separate until it reaches secondary brain areas (Bojsen-Moller and Fahrenkrug, 1971; Eccles, 2000; Kikuta et al., 2008). How the two streams of information are integrated, as well as the functional role of this integration, remain unclear. Because projections from the OB to the OC are sparse and lack apparent topography, it has been a prevalent view that the projections coming from and going out of the OC are random (Bekkers and Suzuki, 2013; Choi et al., 2011; Giessel and Datta, 2014; Haberly, 2001; Illig and Haberly, 2003; Kay, 2011; Rennaker et al., 2007; Schaffer et al., 2018). Contrary to this expectation, we observed that the OC integrates bilateral odor information in a highly non-random way, suggesting a significant degree of order in cortical microcircuits. This suggests that similar information about odor identity is present in each hemisphere of the OC, independent of the nostril sampling the odor.

Importance of the Integration of Bilateral Information

In vision and audition, information from paired sensors (eyes or ears) are combined in the brain to perform specific computations that are behaviorally relevant – for example, estimating distance to or the direction of the source of the stimuli. The existence of two sensors for olfaction has prompted hypotheses about their function (Catania, 2013; Esquivelzeta Rabell et al., 2017; Mainland et al., 2002; Porter et al., 2005; Rajan, 2006). Since the two nostrils may sample independent pockets of air (Eccles, 2000; Kikuta et al., 2008; Wilson and Sullivan, 1999), can bilateral information be used to discover features of the odor stimulus not readily available to single nostrils? Comparison of odor concentration across the two nostrils may aid foraging animals to locate odor sources under conditions where smooth gradients exist (short distances or very still atmospheric conditions) (Catania, 2013; Esquivelzeta Rabell et al., 2017; Gire et al., 2016). This computation requires neurons to be differentially responsive to stimulation of the nostrils, and two brain regions that seem to fulfil this criterion are the AON and APC (Kikuta et al., 2008, 2010; Wilson, 1997). Recent studies have indicated that the AON may be sensitive to the differential activation of left and right nostrils, therefore computing the direction of the stimulus in front of the animal (Esquivelzeta Rabell et al., 2017). Our own data shows that side identity can be decoded from odor responses, which provides further evidence for differential processing (Figure 5D).

In contrast to computations emphasizing the differences between the two sides, many behaviors require common inferences to be made independent of the nostril that is stimulated. One simple example can be found in our everyday life: during a cold, both nostrils are not congested equally. Rather, one nostril is usually more blocked than the other, and which nostril gets clogged changes several times a day (Eccles, 2000). Despite that, we are (fortunately) still able to identify the comforting smell of a chicken soup. In the same fashion, animals need to be able to identify relevant smells like food or a predator, no matter where the odor source is relative to their nose. Indeed, there is evidence for nostril-independent recognition of odors: rats trained to associate odors with reward using only one naris can generalize to stimuli delivered through the other nostril (Kucharski and Hall, 1987, 1988). This behavior requires interhemispheric communication, suggesting a convergence of ipsilateral and contralateral representations in higher brain areas.

Bilateral Integration in the Olfactory Cortex is not Random

Here, we developed and tested a new method to deliver odor stimuli selectively to individual nostrils in awake, freely breathing mice (Figure 2). We performed several experiments to confirm selective stimulation. First, PID recordings indicated that odors were delivered at the same concentration on either side and are not detectable on the side contralateral to the stimulus. Second, direct measurements of sensory input to the olfactory bulb indicated that glomerular responses to contralateral stimulation were below detection threshold. It is possible that some low-level cross contamination went undetected by the PID and glomerular recordings, but it is unlikely that such weak inputs could contribute to contralateral responses that are as strong as those to ipsilateral stimulation. Third, recordings from putative M/T cells in the OB using tetrodes revealed few detectable responses to contralateral nares stimulation. Note that we were unable to replicate the results of a recent publication showing the existence of a large proportion of mirror-symmetric isofunctional M/T cells in the two OBs of the mouse (Grobman et al., 2018). However our observations confirm former work from various teams regarding the near absence of contralateral M/T response in the OB (Kikuta et al., 2008, 2010; Wilson, 1997). Our results are also consistent with the known projections from the AON pars externa to the GABAergic granule cells of the contralateral OB (Schoenfeld and Macrides, 1984; Yan et al., 2008), since any response we saw in M/T cells to contralateral nostril stimulation was inhibitory. The minimal responses in glomeruli and M/T cells also argues strongly against bilateral return of odors from the respiratory system during exhalation.

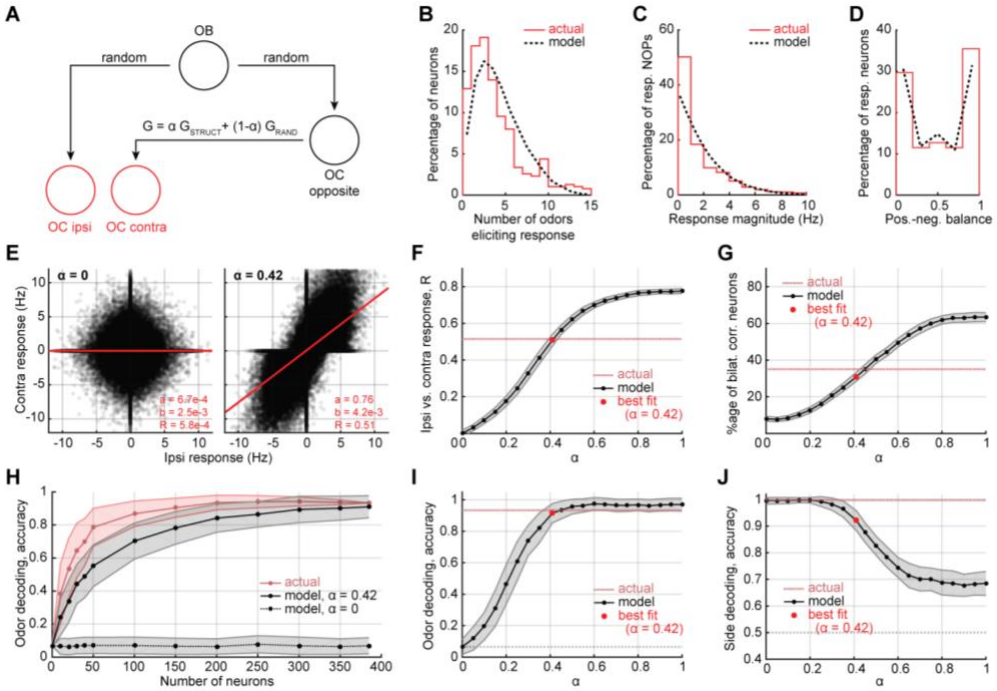

Figure 6: Modeling Olfactory Cross Cortical Connections. (A) Diagram of the model. (B) to (D) Model validation. Contralateral odor responses from the model are overlaid with actual contralateral AON responses (Figures 3E-3G). (E) to (J) Various measurements of cross-cortical alignment from the model. (E) Contra- vs ipsilateral responses for random (alpha = 0) and semi-structured (alpha = 0.42) projections. (F) Contra- vs ipsilateral responses for various alpha values. (G) Percentage of bilaterally-correlated neurons for various alpha values. (H) Odor decoding accuracy for random (alpha = 0) and semi-structured (alpha = 0.42) projections. Red: same as Figure 4B, AON, "test contra". (I) Odor decoding accuracy for various alpha values. (J) Side decoding accuracy for various alpha values. For (E) to (H), measurements from the model were calculated by sampling 385 neurons 200 times. The best fit alpha (0.42) was found by comparing to AON data (n = 385 neurons from 3 mice).

Our first key finding is that responses to the stimulation of the contralateral nostril could readily be detected in all three cortical regions tested (Figure 3). This is not entirely surprising, since crossed projections already occur at the level of the AON and APC, the effects of which can then cascade downstream. Previous studies indicated that contralateral stimulation evoked fewer and weaker responses in

the AON (Kikuta et al., 2008). However, these studies recorded from a small number of neurons in anesthetized animals. While we confirmed the presence of weaker and fewer responses to contralateral stimulations in the AON, the differences were much smaller than previously reported. Another recent study implicated AON in interhemispheric communication using a variety of methods, but the responses of neurons in this area were not measured (Yan et al., 2008). Finally, one previous study reported the presence of neurons responsive to contralateral naris stimulations in the APC of anesthetized rats, but did not test the correlation of the responses between the two nares (Wilson, 1997).

We then found that the odor information arriving ipsilaterally to the OC strongly matches that arriving contralaterally (Figure 4). In particular, we revealed the presence of a sizeable fraction of bilaterally-correlated neurons in the OC. Our results suggest that the bilaterally-correlated neurons are restricted to the AON and APC, which is consistent with the absence of direct bilateral connectivity between the PPCs from both hemispheres (Figure S1A). However, we cannot rule out the possibility that we failed to detect bilaterally-correlated neuron in the PPC because of our limited odor panel and number of repeats. Note that, for the same reasons, our data may underestimate the actual proportion of bilaterally-correlated neurons in the AON and APC. Furthermore, our data offer strong hints that principal neurons are a major part of the ensemble of neurons that have matched responses to stimuli from both nostrils (Figure S3). This feature would allow downstream areas receiving olfactory cortical inputs to readily have access to side-stable odor responses.

We also showed that odor decoding is transferrable across sides (Figure 5). This result by itself was expected, given the presence of matched responses in the OC. However, the fact that a decoder trained with the same set of unilateral responses could decode odor identity from ipsi- and contralateral data with similarly high accuracies was a surprise. It further demonstrated that ipsi- and contralateral odor representations, share a high degree of similarity.

Finally, we considered how the prevalent view of OC connectivity could explain our data (Figure 6). Recent studies have shown that two readouts projected through the same random matrix remain correlated (Babadi and Sompolinsky, 2014; Schaffer et al., 2018). However, these studies do not address alignment due to projections between cortices. Here we implemented a computational model of the olfactory system to test matching of ipsilateral and contralateral odor tuning in the OC as a function of structure in bilateral projections. We showed that, in our model, purely random projections cannot explain our OC results.

Reconciling Our Results with Known Connectivity Schemes

How can the responses of cortical neurons to selective stimulations of the two nostrils be matched? First, there may be topographically matched crossed projection somewhere in the olfactory system allowing bilateral response matching. The only known candidate for such matching is the projection from AON pars externa to OB (Schoenfeld and Macrides, 1984; Yan et al., 2008). This projection, however, should result in net inhibition of M/T cells since its major target are the GABAergic granule cells (Schoenfeld and Macrides, 1984; Yan et al., 2008). Furthermore, previous studies (Kikuta et al., 2008, 2010; Wilson, 1997) and our own data (Figure 2) suggest that this projection is too weak to support the widespread bilateral matching we observed.

A second way in which matched responses may arise is through fine-scale order in anatomical connectivity that somehow allows the same glomerular output channels from both OBs to converge on individual neurons. Such structure seems implausible and has no precedent but remains formally possible.

A third explanation that seems likely because of its simplicity and local nature is that synaptic connectivity in cortical regions is refined by Hebbian plasticity (Best and Wilson, 2003; Franks and Isaacson, 2005; Johenning et al., 2009) to allow matched responses from both sides. During their normal experience, mice will frequently inhale similar odors through both nostrils. This can allow associative plasticity in cortical areas to select for matched inputs from both hemispheres, similar to, for example, the well-studied map development in the visual system (Bednar and Wilson, 2016; Gu and Cang, 2016; Hubel and Wiesel, 1962). This hypothesis of experience-dependent matching of bilateral inputs to individual cortical neurons is open to experimental testing.

Methods

Contact for Reagent and Resource Sharing

Further information and requests for resources and reagents should be directed to and will be fulfilled by the Lead Contact, Venkatesh N. Murthy (vnmurthy@fas.harvard.edu).

Experimental Model and Subject Details

Male C57Bl/6J and OMP-GCaMP3 (Isogai et al., 2011) mice were used in this study. All the mice were 3 to 8 months old at the time of the experiments. Mice were singly housed after chronic tetrode implantation. A summary of the mice used for tetrode recording can be found in Table S1. All experiments were performed in accordance with the guidelines set by the National Institutes of Health and approved by the Institutional Animal Care and Use Committee at Harvard University.

Bilateral Odor Stimulation

The odor panel was composed of 15 monomolecular odors, purchased from Millipore Sigma: isopropyl tiglate, ethyl tiglate, propyl acetate, isoamyl acetate, ethyl valerate, hexanal, heptanal, allyl butyrate, citronellal, hexyl tiglate, 4-allyl anisole, isobutyl propionate, 2-heptanone, ethyl propionate, and eucalyptol (Figure S1A). The odors were diluted in diethyl phthalate, also purchased from Millipore Sigma (final odor dilution: 5% volume/volume). In addition to these 15 odors, we also tested the response to diethyl phthalate alone, referred as the “blank” trials (Methods, “Neuronal Recording” section). The olfactometer was controlled by a custom LabVIEW script (National Instruments).

Odors were delivered through a custom-built facial mask (Figure 2A). The mask was made of a large piece of tubing surrounding the mouse’s muzzle. On each side of the mask, close to each nostril, a piece of tubing delivered odors at a small flow rate (50 standard cubic centimeters per minute). Also on the mask, right below each odor delivery tube, a vacuum ensured proper air cleaning. We confirmed that the mask could deliver similar amounts of odor on each side of the mask with a photoionization detector (miniPID 200B, Aurora Scientific, Canada) (Figure S1B). We confirmed the absence of contralateral stimulations through calcium imaging at the surface of the OB and M/T cell recordings (Figures 1A and 1E).

Odors were delivered for 2s for each trial. To avoid odor habituation, a period of 15s separated consecutive trials (i.e. 15s from the end of a trial to the beginning of the next trial). Each odor was delivered in two configurations: ipsilateral and contralateral to the implantation. Each odor delivery was repeated 7 times. Therefore, each recording session contained $(15\ odors + 1\ blank\ trial) \times 2\ sides \times 7\ repetitions = 224$ odor presentations. The order of odor presentations was randomly shuffled for each recording session.

Breathing Monitoring

The face mask was connected to an airflow sensor (Honeywell AWM3300V, Morris Plains, NJ) to monitor the animal's respiration during the experiments (Figure S1C) and later align neuronal activity with the sniffs (Figure 3C) (Bolding and Franks, 2017). The accuracy of the face mask in monitoring respiration was tested against intranasal pressure transients (Figures S1E-S1H) as described previously (Reisert et al., 2014).

Chronic Tetrode Implantation

Mice were anesthetized with an intraperitoneal injection of ketamine and xylazine (100 mg/kg and 10 mg/kg, respectively), then placed in a stereotaxic apparatus. After the skull was cleaned and gently scratched, a custom-made titanium head bar was glued to it. A small craniotomy was performed above the implantation site, before 8 custom-built tetrodes (Chang et al., 2013) were lowered together into the brain (coordinates for the AON pars principalis: antero-posterior 3mm, medio-lateral 1.5mm, dorso-ventral 2.3mm - APC: antero-posterior 1.6mm, medio-lateral -2.8mm, dorso-ventral 3.4mm - PPC: antero-posterior 0.3mm, medio-lateral 3.9mm, dorso-ventral 3.5mm - OB: antero-posterior 1.2 mm, medio-lateral 1.1 mm, dorso-ventral 0.3mm; all antero-posterior and medio-lateral coordinates are given relative to Bregma, except for the OB, for which they are given relative to the junction of inferior cerebral vein and superior sagittal sinus; all dorso-ventral coordinates are given relative to the brain surface). A reference electrode was implanted on the occipital crest. All the mice were implanted in the right hemisphere, except mouse APC2, which was implanted in the left hemisphere. We did not find any difference between APC2 and the other mice. The whole system was stabilized with dental cement. Mice were given a week of recovery before any new manipulation.

Neuronal Recording

A week after chronic tetrode implantation, mice were progressively habituated to stay calm while head-fixed on the recording setup. The habituation process typically took a week. Brain activity was then recorded once a day, always at the same period of the day, while delivering odors to the ipsilateral or contralateral nostril (Figures 2F and 3A). The mice were awake, head-restrained, and freely-breathing during all the recordings.

Since the tetrode headstage allowed for the tetrodes to be finely adjusted up or down, the tetrodes were slightly lowered in the brain after each recording session (around 40µm deep), ensuring that different neurons were recorded each day.

Electrical activity was amplified, filtered (0.3-6kHz), and digitized at 30kHz (Intan Technologies, RHD2132, connected to an Open Ephys board). Single units were sorted offline manually using MClust script (Schmitzer-Torbert et al., 2005) written for MATLAB (MathWorks). Units with more than 1% of their inter spike intervals below 2ms refractory period were discarded. Units displaying large changes of amplitude or waveform during the recording were also discarded (Rey et al., 2015) (Figures S1G-S1I). The position of the tetrodes in the brain was confirmed post-mortem through electrolesion (200µA for 4s per channel) (Figure S2).

The average response *R* to an odor *o* (in Hz) over the 7 trials *t* was calculated as followed:

$$R = \sum_{t=1}^{7} (Dur_o^t - Bef_o^t)/7 - \sum_{t=1}^{7} (Dur_b^t - Bef_b^t)/7$$

where, for each trial *t*, Dur_o^t (resp. Dur_b^t) is the firing rate during the odor (resp. "blank") delivery, while Bef_o^t (resp. Bef_b^t) is the firing rate before the odor (resp. "blank") delivery.

Dur_o^t (resp. Dur_b^t) was calculated for the first 2s following the first sniff after odor (resp. "blank") onset. Bef_o^t (resp. Bef_b^t) was calculated for the 4s preceding odor (resp. "blank") onset.

To determine the significance of a response to an odor *o* over the 7 trials *t*, we compared the activity evoked by the odor ($Dur_o^t - Bef_o^t$) to the "blank" activity ($Dur_b^t - Bef_b^t$) (Wilcoxon signed-rank test, critical value set to 5%) (Bolding and Franks, 2017).

Acute Calcium Imaging

Mice were anesthetized with an intraperitoneal injection of ketamine/xylazine mixture (100 mg/kg and 10 mg/kg, respectively). After the skull was cleaned and gently scratched, a custom-made titanium head bar was glued to it. A large craniotomy was performed above the two OBs and covered with 1% low melting point agarose (Thermo Fisher). While the mouse was still anesthetized, calcium activity was imaged above the craniotomies with a custom-made epifluorescence microscope (10X objective, Olympus, NA 0.3; blue excitation LED, Thorlabs; emission filter, 500–550nm, Thorlabs; CMOS camera, The Imaging Source) at 4 frames/s, while presenting odors with the custom-built facial mask (Figures 1A and 1B).

The acquired sequences of images were converted to ΔF/F images (change in fluorescence over resting fluorescence). Then the maximal response at each pixel was calculated for each of the 15 odors, for each stimulus configuration (right or left nostrils), and these maximum response maps were used to manually identify glomeruli for further analysis. Finally, for each odor, for each stimulus configuration, the response at each glomerulus was quantified by integrating the ΔF/F signal 4s after odor onset (which corresponds to the 2s of odor presentation, and the 2s immediately following).

Decoding Task

Neuronal Decoding

For each neuron we created a feature vector by calculating the summed spike count in a 2s window after the mouse first sniffs the odor and subtracting from it the same sum from the 'blank' odor averaged across seven trials.

Odor identity decoding ability was assessed using linear classifiers and leave-out cross validation on a pseudopopulation made up of all neurons recorded in a particular cortical area - AON, APC or PPC (Bolding and Franks, 2017). At each instance we chose a particular dataset (either ipsilateral or contralateral odor presentation) and

formed from it a training set by randomly removing one trial per odor. We calculated mean responses for each odor by averaging across the training set. We then chose our test set in two related ways. If we were testing on the same side as we trained (e.g. train ipsilaterally, test ipsilaterally), then the 15 trials (one per odor) outside the training set were used as the test set. If we were testing on the opposite side (e.g. train ipsilaterally, test contralaterally), then one trial per odor from the opposite side was randomly chosen to form the test set. Classification accuracy was measured by assigning each test trial to the closest Euclidean mean odor response and calculating the percentage of trials correctly assigned (Bolding and Franks, 2017). This process was repeated 200 times using different random test and train trial choices.

In order to examine the effect of changing number of neurons on classification accuracy, we randomly selected neurons from the pseudopopulation and performed classification using only the selected cells. This process is repeated 200 times. We then report the average accuracy and standard deviation over those 200 selections of neurons and, for each set of neurons, 200 sets of train/test trials in Figures 5 and S5.

A very similar process is employed for side decoding. One trial per side was removed, the remaining trials are averaged to form a mean side response for both ipsilateral and contralateral presentations. The removed trials are then classified to the nearer mean side response and accuracy is the percentage correctly assigned. This is repeated 200 times for different random removed trial choices.

Comparisons to the Theoretical Model

Our model predicts the trial-averaged neural responses. In order to make comparisons to the neuronal data, we designed a new classification task. For simulations and trial averaged neuronal data we performed odor decoding as follows: we assigned each of the 15 odor centroids from one side (contralateral or ipsilateral) to their closest neighbor on the other side. This classification was correct if an odor from one side was classified to the same odor on the other side. The accuracy is then the proportion of odors correctly assigned. Again, average accuracy and standard deviation over 200 randomly chosen neurons are reported in Figures 5 and S5. One exception to the procedure above is Figure S4G, right panel, where we classify centroids to their nearest angular neighbor.

For side classification comparisons, the two centroids corresponding to a given odor presented on both sides are removed. From the remaining 28 centroids, two points representing ipsilateral and contralateral cortex are made by averaging over all remaining centroids from a particular side. The two points we removed are then classified as ipsilateral or contralateral depending on which mean they are nearest to. This procedure is repeated 15 times, removing a different odor each time. We report the average accuracy and standard deviation over 200 randomly chosen pseudopopulations in Figures 5 and S5.

Computational Modeling

We built a feed-forward neural network model to explore the implications of a random or structured connection between the olfactory cortex in each hemisphere. We effectively model one cortical region in each hemisphere, based on the AON.

To begin, we considered the cortical response to odors presented ipsilaterally, later we will link these to explore interhemispheric effects. Each cortical neuron's activity to an ipsilateral odor o is a weighted sum of glomerular activities passed through an activation function:

$$y_{o,i} = \mathrm{f}\left(\Sigma_{j=1}^{N_x} J_{ij} x_{o,j}\right) = \mathrm{f}\left(\mathrm{h}_{\mathrm{o,i}}\right),$$

where **J** is the glomerular to cortical connectivity matrix, $x_{o,j}$ *and* $y_{o,i}$ are the firing rates of glomerulus j and cortical neuron i respectively to odor o, $\mathrm{h}_{\mathrm{o,i}}$ is the input to cortical neuron i, j runs from 1 to N_x (the total number of glomeruli), and f is the activation function.

The zero point of these neurons is set to be basal firing rate plus response to a blank odor. Therefore, we modeled only odor related perturbations from the blank and base to match all comparisons to the blank and base subtracted data.

The nonlinearity, f, was chosen to recreate features of the electrophysiological recordings. First, it was found that the odor related perturbations are equally likely to be positive or negative (Of all the significant neuron-odor pairs, 46% are positive in the AON, 48% in the APC, and 48% in the PPC) therefore we chose a nonlinearity that was symmetric around zero. Negative activity does not mean the neurons have a negative firing rate, but that their firing rate is inhibited relative to their response to base plus blank. Second, consistent with previous findings (Bolding and Franks, 2017; Iurilli and Datta, 2017; Poo and Isaacson, 2009), the cortical response to odors was relatively sparse. Therefore, we chose the shrink function:

$$f\left(h_{o,i}\right) = \begin{cases} h_{o,i} - \varphi & if \quad h_{o,i} \geq \varphi \\ 0 & if \quad \left|h_{o,i}\right| < \varphi \\ h_{o,i} + \varphi & if \quad h_{o,i} \leq \varphi \end{cases},$$

where ϕ is a threshold that controls sparseness.

Based on previous work we then modelled the connectivity matrix between the bulb and the cortex to be completely random (Schaffer et al., 2018) with elements either equal to 0, with probability $1 - \xi$, or drawn independently from a zero mean distribution with finite variance $\frac{\sigma^2}{N_x}$, with probability ξ. ξ, therefore, controls the sparseness of the matrix[1]. Now by Central Limit Theorem $\mathrm{h}_{\mathrm{o,i}}$ is distributed in a Gaussian manner and with zero mean.

Since input to each cortical neuron is statistically independent, to fully specify its distribution, we must simply set the odor-odor covariance matrix of the Gaussian. Under the assumption that the size of the OB output response is identical for each odor ($|\boldsymbol{x_o}|^2 = |\boldsymbol{x_{o'}}|^2$ ∀ odors o and o'), which can be justified by the divisive normalization that appears to happen in the OB (Banerjee et al., 2015; Zhu et al., 2013), the elements of the covariance matrix can be found as follows:

$$\mathbb{E}_i\left[h_{o,i}^2\right] = \xi\sigma^2 \frac{1}{N_x} |\boldsymbol{x_o}|^2 = \gamma^2$$

$$\mathbb{E}_i\left[h_{o,i} h_{o',i}\right] = \xi\sigma^2 \frac{1}{N_x} \boldsymbol{x_o} . \boldsymbol{x_{o'}} = \gamma^2 \cos\left(\theta_{o,o'}\right),$$

where $\mathbb{E}_i$ refers to an expectation over the cortical population and we

1 Note that negative weights do not mean that OB inputs are directly inhibitory; they rather model OB inputs projecting to inhibitory OC neurons, which in turn project to our OC neurons of interest.

defined a new variable $\gamma^2 := \xi\sigma^2 \frac{1}{N_x}|\boldsymbol{x_o}|^2$ that controls the variance, and $\theta_{o,o'}$ is the angle between two glomerular representations. For the 15 odors under consideration we used calcium imaging to extract the cosine similarity which serves as the Gaussian covariance. To complete our ipsilateral specification we must, therefore, only choose γ and a threshold ϕ – we shall rationalize these terms in two ways.

The threshold controls sparseness of cortical response, this we match to the AON recordings. The sparseness of the recordings is measured as the proportion of neuron-odor pairs for which the Wilcoxon signed rank test p value comparing the set of seven trials to mean blank odor response is below 5% (22.4% Ipsilateral, 25.2% Contralateral). Labeling the sparseness as S, because of the assumed Gaussianity of cortical inputs, we get:

$$\mathrm{S} = \frac{1}{\sqrt{2\pi\gamma^2}}\left(\int_{\phi}^{\infty} \mathrm{e}^{-\frac{\mathrm{h}^2}{2\gamma^2}}\,\mathrm{dh} + \int_{-\infty}^{-\phi} \mathrm{e}^{-\frac{\mathrm{h}^2}{2\gamma^2}}\,\mathrm{dh}\right) = \mathrm{erfc}\left[\frac{\phi}{\gamma\sqrt{2}}\right],$$

where erfc is the cumulative error function. Therefore, the sparseness sets the ratio of threshold to variance:

$$\frac{\phi}{\gamma} = \sqrt{2}\mathrm{erfc}^{-1}[S].$$

Finally, we use the ipsilateral distribution of significant response magnitudes in the AON (Figure 3E, top panel) to fit the conversion of numbers to firing rate (Hz), γ. Our model predicts the significant response magnitude distribution to be the tail of a Gaussian, by changing γ we are simply rescaling the x axis of this distribution, we choose the γ that permits the best model-data fit. This fully specified the ipsilateral simulations, and fit the data remarkably well (see Figures 6 and S7).

To compare ipsilateral to contralateral responses we create two ipsilateral responses according to the scheme above. One of these is then mapped through a cross cortical connectivity matrix to create a contralateral response. We use this contralateral response and the second ipsilateral creation for our comparisons to mice.

Our final task, therefore, is to design a cross cortical connectivity matrix. In order to explore the implications of random and structured connections we combined two different cross cortical connectivity matrices.

There is a random component whose elements are drawn from a zero mean normal distribution with variance 1 (this choice of variance is unimportant as the matrix will be rescaled in future):

$$\mathrm{G}_{\mathrm{ij}}^{\mathrm{Rand}} \sim \mathcal{N}(0,1) \text{ with probability } \xi\text{, else 0.}$$

And there is a structured Hebbian component from contralateral to ipsilateral (Dayan and Abbott, 2001):

$$G_{Struct}^{Unscaled} = \sum_{\mathrm{o}=1}^{\mathrm{P}} \left(\mathbf{Y_o^{Ipsi}} - \mathbf{C^{Ipsi}}\right)\left(\mathbf{Y_o^{Opp}} - \mathbf{C^{Opp}}\right)^{\mathbf{T}},$$

where $\mathbf{Y_o^{Ipsi}}$ is the response vector to odor o presented ipsilaterally in the ipsilateral cortex, $\mathbf{C^{Ipsi}}$ is response in the ipsilateral cortex averaged over odors, P=15 is the total number of odors, and $\mathbf{Y_o^{Opp}}$ is the response in the opposite cortex to an odor presented in the opposite nostril.

These two matrices currently have outputs that are of arbitrary magnitudes. To ensure each contribution has a roughly similar sized output, the structured section is rescaled by a factor:

$$\mathrm{G_{Struct}} = \chi\, \mathrm{G_{Struct}^{Unscaled}} \text{ where } \chi = \frac{\Sigma_{\mathrm{o}=1}^{\mathrm{P}}\left|\mathrm{G_{Rand}Y_o^{Opp}}\right|}{\Sigma_{\mathrm{o}=1}^{\mathrm{P}}\left|\mathrm{G_{Struct}^{Unscaled}Y_o^{Opp}}\right|},$$

before being combined using the parameter α to create a cross cortical link with varying levels of randomness/structure:

$$G = \alpha \mathrm{G_{Struct}} + (1-\alpha)\mathrm{G_{Rand}}.$$

Since the size of the outputs of each matrix are equal, we can now interpret alpha as the proportion of contralateral input magnitude that is formed by structured connectivity.

The magnitude of the elements of this matrix are then scaled again such that the resulting contralateral representation has the desired sparseness when the same piriform threshold is applied as was used to create the ipsilateral sparseness. Finally, the conversion to Hz, γ, is used to compare to data.

We varied alpha and looked at how four measures of cross-cortical alignment changed (Figures 6E-6J; see main text for details) and how simulations compared to our actual AON data. We chose the optimal alpha to be the point with the minimum z^2-score across the four – the smallest squared sum of sigmas (error bars) between the point and the AON data line in all four plots.

We modeled our AON with 50,000 neurons, this is a rough underestimate based on other paleocortical neuronal densities (Srinivasan and Stevens, 2017) and measurements of AON size from the Allen Brain Atlas. Our model, however, was robust to changes in number of neurons, for example we tried a 25,000 neuron version (Figures S7E-S7H) and the optimal alpha did not change.

Quantification and Statistical Analysis

All quantifications and statistical analyses were performed using custom scripts in MATLAB (MathWorks), except (1) the circular statistical analyses, which were performed with the CircStat toolbox written by Philipp Berens (Berens, 2009), and (2) the Hartigan's dip tests, which were performed with the code written by Ferenc Mechler (Mechler and Ringach, 2002). The linear regressions were obtained with the least square method. The data is given as median ± standard deviation (SD), unless specified otherwise. For all statistical tests, the critical value was set to 5%. All statistical tests were two-sided, with the exception of the bootstrap strategies (where we asked whether the measurements were significantly higher than chance).

Additionally, the significance of the linear regressions was tested using either an F-test (Figures 4, S3, and S4). The significance of the percentage of bilaterally-correlated neurons was tested using a bootstrap strategy (see figure caption for details). Table S2 summarizes all the statistical tests performed in this study.

Lead Contact and Materials Availability

All data and code used to compute quantities presented in this study is available on the Murthy lab GitHub repository page: https://github.com/VNMurthyLab.

Author Contributions

V.N.M and J.G designed the experimental setup. C.P and W.D. designed the computational modeling strategy with inputs from all authors. J.G. acquired the electrophysiological data. J.G. and W.D. analyzed the data. J.G. and W.D. wrote the manuscript with inputs

form all authors.

Acknowledgements

Research reported in this paper was supported, in part, by grants from the NIH (R01 DC016289, R01DC011291), the Harvard Merit Fellowship, and the Herchel Smith Scholarship. We thank Vikrant Kapoor, as well as all members of the Murthy and Pehlevan labs for helpful feedback. We also thank Massimo Vergassola and Gautam Reddy for critical discussion. Finally, we thank Naoshige Uchida and Kenneth Blum for their precious feedback on a previous version of this manuscript.

Competing Interests

The authors declare no competing interests.

Reference

Babadi, B., and Sompolinsky, H. (2014). Sparseness and Expansion in Sensory Representations. Neuron.

Banerjee, A., Marbach, F., Anselmi, F., Koh, M.S., Davis, M.B., Garcia da Silva, P., Delevich, K., Oyibo, H.K., Gupta, P., Li, B., et al. (2015). An Interglomerular Circuit Gates Glomerular Output and Implements Gain Control in the Mouse Olfactory Bulb. Neuron.

Bednar, J.A., and Wilson, S.P. (2016). Cortical Maps. Neuroscientist.

Bekkers, J.M., and Suzuki, N. (2013). Neurons and circuits for odor processing in the piriform cortex. Trends Neurosci. *36*, 429–438.

Berens, P. (2009). CircStat : A MATLAB Toolbox for Circular Statistics . J. Stat. Softw.

Best, A.R., and Wilson, D.A. (2003). A postnatal sensitive period for plasticity of cortical afferents but not cortical association fibers in rat piriform cortex. Brain Res. *961*, 81–87.

Bojsen-Moller, F., and Fahrenkrug, J. (1971). Nasal swell-bodies and cyclic changes in the air passage of the rat and rabbit nose. J. Anat. *110*, 25–37.

Bolding, K.A., and Franks, K.M. (2017). Complementary codes for odor identity and intensity in olfactory cortex. Elife *6*.

Bolding, K.A., and Franks, K.M. (2018). Recurrent cortical circuits implement concentration-invariant odor coding. Science (80-.).

Boyd, A.M., Sturgill, J.F., Poo, C., and Isaacson, J.S. (2012). Cortical Feedback Control of Olfactory Bulb Circuits. Neuron *76*, 1161–1174.

Brewer, A.A., and Barton, B. (2016). Maps of the Auditory Cortex. Annu. Rev. Neurosci.

Caron, S.J.C., Ruta, V., Abbott, L.F., and Axel, R. (2013). Random convergence of olfactory inputs in the Drosophila mushroom body. Nature.

Catania, K.C. (2013). Stereo and serial sniffing guide navigation to an odour source in a mammal. Nat. Commun. *4*, 1441.

Chang, E.H., Frattini, S.A., Robbiati, S., and Huerta, P.T. (2013). Construction of Microdrive Arrays for Chronic Neural Recordings in Awake Behaving Mice. J. Vis. Exp.

Choi, G.B., Stettler, D.D., Kallman, B.R., Bhaskar, S.T., Fleischmann, A., and Axel, R. (2011). Driving opposing behaviors with ensembles of piriform neurons. Cell.

Davison, I.G., and Ehlers, M.D. (2011). Neural Circuit Mechanisms for Pattern Detection and Feature Combination in Olfactory Cortex. Neuron.

Dayan, P., and Abbott, L.F. (2001). Theoretical Neuroscience: Computational and Mathematical Modeling of Neural Systems.

Eccles, R. (2000). Nasal airflow in health and disease. Acta Otolaryngol. *120*, 580–595.

Esquivelzeta Rabell, J., Mutlu, K., Noutel, J., Martin del Olmo, P., and Haesler, S. (2017). Spontaneous Rapid Odor Source Localization Behavior Requires Interhemispheric Communication. Curr. Biol. *27*, 1542-1548.e4.

Frank, L.M., Brown, E.N., and Wilson, M.A. (2001). A comparison of the firing properties of putative excitatory and inhibitory neurons from CA1 and the entorhinal cortex. J. Neurophysiol.

Franks, K.M., and Isaacson, J.S. (2005). Synapse-specific downregulation of NMDA receptors by early experience: A critical period for plasticity of sensory input to olfactory cortex. Neuron *47*, 101–114.

Ghosh, S., Larson, S.D., Hefzi, H., Marnoy, Z., Cutforth, T., Dokka, K., and Baldwin, K.K. (2011). Sensory maps in the olfactory cortex defined by long-range viral tracing of single neurons. Nature.

Giessel, A.J., and Datta, S.R. (2014). Olfactory maps, circuits and computations. Curr. Opin. Neurobiol. *24*, 120–132.

Gire, D.H., Kapoor, V., Arrighi-Allisan, A., Seminara, A., and Murthy, V.N. (2016). Mice develop efficient strategies for foraging and navigation using complex natural stimuli. Curr. Biol. *26*, 1261–1273.

Grobman, M., Dalal, T., Lavian, H., Shmuel, R., Belelovsky, K., Xu, F., Korngreen, A., and Haddad, R. (2018). A Mirror-Symmetric Excitatory Link Coordinates Odor Maps across Olfactory Bulbs and Enables Odor Perceptual Unity. Neuron.

Gu, Y., and Cang, J. (2016). Binocular matching of thalamocortical and intracortical circuits in the mouse visual cortex. Elife.

Gur, M., Beylin, a, and Snodderly, D.M. (1999). Physiological properties of macaque V1 neurons are correlated with extracellular spike amplitude, duration, and polarity. J. Neurophysiol. *82*, 1451–1464.

Haberly, L.B. (2001). Parallel-distributed processing in olfactory cortex: new insights from morphological and physiological analysis of neuronal circuitry. Chem. Senses *26*, 551–576.

Haberly, L.B., and Price, J.L. (1978). Association and commissural fiber systems of the olfactory cortex of the rat. J. Comp. Neurol. *178*, 711–740.

Harding-Forrester, S., and Feldman, D.E. (2018). Somatosensory maps. In Handbook of Clinical Neurology, p.

Hassani, O.K., Lee, M.G., Henny, P., and Jones, B.E. (2009). Discharge Profiles of Identified GABAergic in Comparison to Cholinergic and Putative Glutamatergic Basal Forebrain Neurons across the Sleep-Wake Cycle. J. Neurosci. *29*, 11828–11840.

Hu, R., Zhang, J., Luo, M., and Hu, J. (2017). Response Patterns of GABAergic Neurons in the Anterior Piriform Cortex of Awake Mice. Cereb. Cortex *27*, 3110–3124.

Hubel, D.H., and Wiesel, T.N. (1962). Receptive fields, binocular interaction and functional architecture in the cat's visual cortex. J. Physiol.

Illig, K.R., and Haberly, L.B. (2003). Odor-evoked activity is spatially distributed in piriform cortex. J. Comp. Neurol. *457*, 361–373.

Isogai, Y., Si, S., Pont-Lezica, L., Tan, T., Kapoor, V., Murthy, V.N., and Dulac, C. (2011). Molecular organization of vomeronasal chemoreception. Nature *478*, 241–245.

Iurilli, G., and Datta, S.R. (2017). Population Coding in an Innately Relevant Olfactory Area. Neuron.

Johenning, F.W., Beed, P.S., Trimbuch, T., Bendels, M.H.K., Winterer, J., and Schmitz, D. (2009). Dendritic compartment and neuronal output mode determine pathway-specific long-term potentiation in the piriform cortex. J. Neurosci. *29*, 13649–13661.

Kaas, J.H. (1997). Topographic maps are fundamental to sensory processing. Brain Res. Bull.

Kay, L.M. (2011). Olfactory coding: Random scents make sense. Curr. Biol.

Kikuta, S., Kashiwadani, H., and Mori, K. (2008). Compensatory rapid switching of binasal inputs in the olfactory cortex. J. Neurosci. *28*, 11989–11997.

Kikuta, S., Sato, K., Kashiwadani, H., Tsunoda, K., Yamasoba, T., and Mori, K. (2010). Neurons in the anterior olfactory nucleus pars externa detect right or left localization of odor sources. Proc. Natl. Acad. Sci. *107*, 12363–12368.

Kucharski, D., and Hall, W.G. (1987). New routes to early memories. Science (80-.). *238*, 786–788.

Kucharski, D., and Hall, W.G. (1988). Developmental Change in the Access to Olfactory Memories. Behav. Neurosci.

Litaudon, P., Amat, C., Bertrand, B., Vigouroux, M., and Buonviso, N. (2003). Piriform cortex functional heterogeneity revealed by cellular responses to odours. Eur. J. Neurosci.

Mainland, J.D., Bremner, E. a, Young, N., Johnson, B.N., Khan, R.M., Bensafi, M., and Sobel, N. (2002). Olfactory plasticity: one nostril knows what the other learns. Nature *419*, 802.

Mechler, F., and Ringach, D.L. (2002). On the classification of simple and complex cells. Vision Res.

Miyamichi, K., Amat, F., Moussavi, F., Wang, C., Wickersham, I., Wall, N.R., Taniguchi, H., Tasic, B., Huang, Z.J., He, Z., et al. (2011). Cortical representations of olfactory input by trans-synaptic tracing. Nature *472*, 191–196.

Mori, K. (1999). The Olfactory Bulb: Coding and Processing of Odor Molecule Information. Science (80-.). *286*, 711–715.

Murthy, V.N. (2011). Olfactory maps in the brain. Annu. Rev. Neurosci. *34*, 233–258.

Nagayama, S., Homma, R., and Imamura, F. (2014). Neuronal organization of olfactory bulb circuits. Front. Neural Circuits *8*.

Nauhaus, I., and Nielsen, K.J. (2014). Building maps from maps in primary visual cortex. Curr. Opin. Neurobiol.

Otazu, G.H., Chae, H., Davis, M.B., and Albeanu, D.F. (2015). Cortical Feedback Decorrelates Olfactory Bulb Output in Awake Mice. Neuron *86*, 1461–1477.

Poo, C., and Isaacson, J.S. (2009). Odor Representations in Olfactory Cortex: "Sparse" Coding, Global Inhibition, and Oscillations. Neuron.

Porter, J., Anand, T., Johnson, B., Khan, R.M., and Sobel, N. (2005). Brain mechanisms for extracting spatial information from smell. Neuron *47*, 581–592.

Povysheva, N. V., Gonzalez-Burgos, G., Zaitsev, A. V., Kröner, S., Barrionuevo, G., Lewis, D.A., and Krimer, L.S. (2006). Properties of excitatory synaptic responses in fast-spiking interneurons and pyramidal cells from monkey and rat prefrontal cortex. Cereb. Cortex *16*, 541–552.

Rajan, R. (2006). Rats Smell in Stereo. Science (80-.). *311*, 666–670.

Reisert, J., Golden, G.J., Matsumura, K., Smear, M., Rinberg, D., and Gelperin, A. (2014). Comparing thoracic and intra-nasal pressure transients to monitor active odor sampling during odor-guided decision making in the mouse. J. Neurosci. Methods *221*, 8–14.

Rennaker, R.L., Chen, C.-F.F., Ruyle, A.M., Sloan, A.M., and Wilson, D.A. (2007). Spatial and Temporal Distribution of Odorant-Evoked Activity in the Piriform Cortex. J. Neurosci. *27*, 1534–1542.

Rey, H.G., Pedreira, C., and Quian Quiroga, R. (2015). Past, present and future of spike sorting techniques. Brain Res. Bull. *119*, 106–117.

Schaffer, E.S., Stettler, D.D., Kato, D., Choi, G.B., Axel, R., and Abbott, L.F. (2018). Odor Perception on the Two Sides of the Brain: Consistency Despite Randomness. Neuron.

Schmitzer-Torbert, N., Jackson, J., Henze, D., Harris, K., and Redish, A.D. (2005). Quantitative measures of cluster quality for use in extracellular recordings. Neuroscience *131*, 1–11.

Schoenfeld, T.A., and Macrides, F. (1984). Topographic organization of connections between the main olfactory bulb and pars externa of the anterior olfactory nucleus in the hamster. J. Comp. Neurol. *227*, 121–135.

Scott, J.W., McBride, R.L., and Schneider, S.P. (1980). The organization of projections from the olfactory bulb to the piriform cortex and olfactory tubercle in the rat. J. Comp. Neurol. *194*, 519–534.

Sosulski, D.L., Lissitsyna Bloom, M., Cutforth, T., Axel, R., and Datta, S.R. (2011). Distinct representations of olfactory information in different cortical centres. Nature *472*, 213–216.

Soucy, E.R., Albeanu, D.F., Fantana, A.L., Murthy, V.N., and Meister, M. (2009). Precision and diversity in an odor map on the olfactory bulb. Nat. Neurosci. *12*, 210–220.

Srinivasan, S., and Stevens, C.F. (2017). A quantitative description of the mouse piriform cortex. BioRxiv 99002.

Strotmann, J., Conzelmann, S., Beck, a, Feinstein, P., Breer, H., and Mombaerts, P. (2000). Local permutations in the glomerular array of the mouse olfactory bulb. J. Neurosci. *20*, 6927–6938.

Suzuki, S.S., and Smith, G.K. (1985). Burst characteristics of hippocampal complex spike cells in the awake rat. Exp. Neurol. *89*, 90–95.

Swadlow, H.A. (2003). Fast-spike Interneurons and Feedforward Inhibition in Awake Sensory Neocortex. Cereb. Cortex *13*, 25–32.

Weir, K., Blanquie, O., Kilb, W., Luhmann, H.J., and Sinning, A. (2015). Comparison of spike parameters from optically identified GABAergic and glutamatergic neurons in sparse cortical cultures. Front. Cell. Neurosci. *8*.

Wilson, D.A. (1997). Binaral interactions in the rat piriform cortex. J Neurophysiol *78*, 160–169.

Wilson, D.A., and Sullivan, R.M. (1999). Respiratory airflow pattern at the rat's snout and an hypothesis regarding its role in olfaction. Physiol. Behav. *66*, 41–44.

Wilson, D.A., and Sullivan, R.M. (2011). Cortical processing of odor objects. Neuron *72*, 506–519.

Yan, Z., Tan, J., Qin, C., Lu, Y., Ding, C., and Luo, M. (2008). Precise Circuitry Links Bilaterally Symmetric Olfactory Maps. Neuron *58*, 613–624.

Zhan, C., and Luo, M. (2010). Diverse patterns of odor representation by neurons in the anterior piriform cortex of awake mice. J. Neurosci. *30*, 16662–16672.

Zhu, P., Frank, T., and Friedrich, R.W. (2013). Equalization of odor representations by a network of electrically coupled inhibitory interneurons. Nat. Neurosci.